Pressure and magnetic field tuned quantum critical point in the Kondo antiferromagnet CePtZn

2009 J. Phys.: Condens. Matter 21 156001

(http://iopscience.iop.org/0953-8984/21/15/156001)

J. Phys.: Condens. Matter **21** (2009) 156001 (8pp) doi:10.1088/0953-8984/21/15/156001

Pressure and magnetic field tuned quantum critical point in the Kondo antiferromagnet CePtZn

S K Dhar[1], R Kulkarni[1], H Hidaka[2], Y Toda[2], H Kotegawa[2,5], T C Kobayashi[2], P Manfrinetti[3,4] and A Provino[3]

[1] CMP&MS, TIFR, Homi Bhabha Road, Colaba, Mumbai 400 005, India
[2] Graduate School of Natural Science and Technology, Okayama University, Okayama 700-8530, Japan
[3] Dipartimento di Chimica e Chimica Industriale, Università di Genova, Via Dodecaneso 31, 16146 Genova, Italy
[4] LAMIA Laboratory-CNR-INFM, Corso Perrone 24, 16152 Genova, Italy

Received 1 December 2008, in final form 30 January 2009
Published 17 March 2009
Online at stacks.iop.org/JPhysCM/21/156001

Abstract

We report magnetization, heat capacity and electrical resistivity measurements on CePtZn, which crystallizes in the orthorhombic TiNiSi type structure. Magnetization and electrical resistivity on the iso-structural series of compounds $Ce_{1-x}La_xPtZn$ ($x = 0.1$, 0.2 0.5 and 1) were also carried out. The electrical resistivity of CePtZn was also measured in external magnetic fields up to 12 T and under pressures up to 2.66 GPa. We find that CePtZn is a dense Kondo lattice, ordering antiferromagnetically at $T_N = 1.7$ K, with a comparable Kondo temperature. The magnetic transition temperature, T_N, is continuously suppressed both by the magnetic field and pressure and $T_N \to 0$ around 5–6 T and at 1.2 GPa, respectively. Non-Fermi liquid behavior of resistivity at 4 T and 1.2 GPa and logarithmic divergence of the heat capacity, C_{4f}/T, at 6 T in a limited temperature region strongly suggest the emergence of a quantum critical point as $T_N \to 0$.

(Some figures in this article are in colour only in the electronic version)

1. Introduction

Cerium and ytterbium based compounds are studied extensively as they provide us with systems displaying a variety of behaviors arising from strong electron correlations, such as heavy fermions and unconventional superconductivity, anomalous magnetic ordering, quantum critical points and non-Fermi liquid behavior, etc. Recently, YbPtZn crystallizing in the orthorhombic TiNiSi type structure has been shown to be a dense Kondo lattice ordering magnetically at 1.35 K [1]. A reduced magnetic entropy of just 1.6 J mol^{-1} K^{-1} up to the ordering temperature, and a large (0.75 J mol^{-1} K^{-2}) coefficient of the linear term in the electronic specific heat γ in the magnetically ordered state of YbPtZn provide evidence for a strongly renormalized electronic state due to the Kondo interaction. Heat capacity data in applied fields and magnetoresistivity indicated a ferromagnetic interaction between the Yb ions, which is rather uncommon. Since the $4f^{13}$-Yb^{3+} and $4f^1$-Ce^{3+} electronic configurations are often viewed as mirror analogs of each other, it was of interest to investigate the magnetic behavior of the iso-structural CePtZn discovered in the course of our work [1]. In this paper we show that CePtZn, like its Yb-counterpart, is a dense Kondo lattice, ordering antiferromagnetically at $T_N = 1.7$ K. The relatively low T_N of CePtZn and its Kondo behavior at ambient pressure motivated us to study the effect of externally applied magnetic fields and hydrostatic pressure on the interplay between the magnetic ordering and the strongly correlated electronic ground states. We find that T_N is continuously shifted to lower temperatures in applied magnetic fields and by pressure, resulting in $T_N \to 0$ at 5–6 T and 1.2 GPa, respectively. The non-Fermi liquid temperature dependence of the electrical resistivity, $\Delta\rho \propto T^n$, $1 \leqslant n \leqslant 2$, at 4 T and 1.2 GPa and the logarithmic divergence of the heat capacity, C_{4f}/T, at 6 T in a limited range of

[5] Present address: Department of Physics, Graduate School of Science, Kobe University, 1-1 Rokko-dai, Nada Kobe, 657-8501, Japan.

Table 1. Thermal treatment, lattice constants (from Guinier powder pattern), unit cell volume V_U and mean atomic volume V_{at}, for $Ce_{1-x}La_xPtZn$ compounds (orthorhombic TiNiSi type, o$P12$-$Pnma$).

Compound	Thermal treatment	Lattice constants			V_U	V_{at}
		a (Å)	b (Å)	c (Å)	(Å^3)	(Å^3)
LaPtZn	800 °C—5 days	7.192(2)	4.384(1)	8.160(3)	256.82	21.40
$Ce_{0.5}La_{0.5}PtZn$	800 °C—7 days	7.129(2)	4.375(1)	8.128(2)	253.53	21.13
$Ce_{0.8}La_{0.2}PtZn$	800 °C—7 days	7.098(1)	4.367(1)	8.116(2)	251.56	20.96
$Ce_{0.9}La_{0.1}PtZn$	800 °C—7 days	7.083(2)	4.364(1)	8.104(2)	250.49	20.87
CePtZn	800 °C—8 days	7.074(2)	4.360(1)	8.104(1)	249.94	20.83

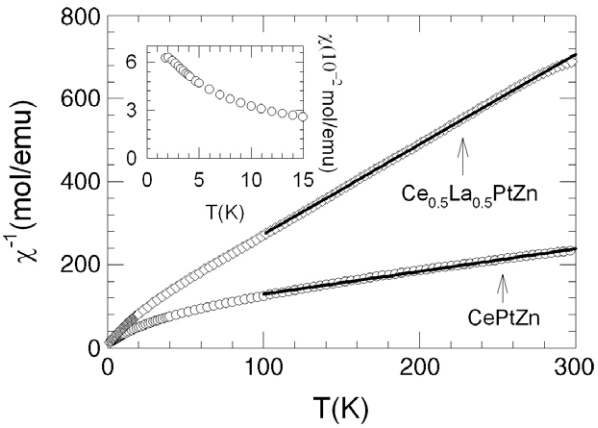

Figure 1. The inverse susceptibility of CePtZn and $Ce_{0.5}La_{0.5}PtZn$ between 1.8 and 300 K. The solid lines are fits of the modified Curie–Weiss expression to the data. The inset shows the susceptibility of CePtZn below 15 K.

temperature suggest the appearance of a quantum critical point (QCP) as $T_N \to 0$. We do not observe any signature of superconductivity up to the highest applied pressure of 2.66 GPa in our experiments.

2. Experimental details

The preparation of CePtZn followed a procedure similar to that of YbPtZn described in [1]. Briefly, CePtZn, non-magnetic reference analog LaPtZn and solid solutions $Ce_{1-x}La_xPtZn$ for $x = 0.1$, 0.2 and 0.5 were prepared in sealed, out-gassed tantalum crucibles in a high frequency induction furnace due to the high vapor pressure of zinc. The purity of metals used was 99.9 wt% for La, 99.95 wt% for Ce and 99.99 wt% for Pt and Zn. The alloys, melted in the temperature range 1500–1600 °C, were slowly cooled and then annealed at 800 °C for 5–10 days.

Metallographic examination was performed by both optical and electron microscopy; semi-quantitative phase analysis by an electron probe micro-analyzer was carried out on some samples. Powder patterns of the annealed samples were obtained on a Guinier–Stoe camera using Cu Kα_1 radiation and pure Si as an internal standard (a = 5.4308 Å). Indexing of the observed patterns was carried out by a direct comparison with those calculated using the LAZY PULVERIX [2] program and the lattice parameters then determined by the least squares method.

The magnetization was measured in a superconducting quantum interference device (Quantum Design). Zero field heat capacity data down to 0.4 K and in-field data down to 1.8 K, and resistivity data down to 1.8 K in zero and applied fields up to 12 T were taken using a Physical Property Measuring System (Quantum Design). Resistivity data down to about 60 mK in zero and applied fields up to 8 T were taken in a dilution refrigerator. The resistivity was also measured under pressure up to 2.66 GPa using an indenter type pressure cell [3]. The pressure-transmitting medium was Daphne oil (7373). The pressure was determined by measuring the superconducting transition temperature on a lead manometer.

3. Results and discussion

Metallographic examination showed that the samples were single, or nearly single, phase alloys containing negligible amounts of secondary phases (<1–2%) as grain boundaries. The Guinier patterns were easily and well indexed, on the basis of the orthorhombic TiNiSi type structure and assuming the same atomic positions as determined earlier for YbPtZn, by single crystal data [1]. The lattice parameters are listed in table 1. The variation of the mean atomic volume V_{at} (unit cell volume divided by the total number of atoms) in $Ce_{1-x}La_xPtZn$ follows a linear trend with x in accordance with Vegard's law. Our values for the lattice parameters of CePtZn are in close agreement with those reported by Mishra *et al* [4].

Figure 1 depicts the inverse susceptibility χ^{-1} of CePtZn, measured in an applied field of 0.3 T, plotted against the temperature T. Typically, the susceptibility of cerium compounds in the paramagnetic region, sufficiently far above the magnetic transition temperature, follows the Curie–Weiss behavior, such that $\chi = C_{cw}/(T-\theta_p)$. Here C_{cw} is the effective Curie constant of the Ce ions and θ_p is the paramagnetic Curie temperature. However, χ^{-1} in CePtZn does not vary linearly with temperature and it instead exhibits a gentle curvature right up to 300 K. A strong magnetic anisotropy arising due to crystal electric fields (CEF), which gives rise to Curie–Weiss behavior of the magnetic susceptibility along the easy direction of magnetization and a weakly temperature dependent susceptibility along the hard direction, can be a possible cause of the curvature in χ^{-1} versus temperature. In such cases, a modified Curie–Weiss expression is often used that includes a temperature independent susceptibility term χ_0. Such a procedure applied to CePtZn yields a good fit to the data, but the fit parameters show a minor variation with the temperature range of the fit; e.g. effective paramagnetic

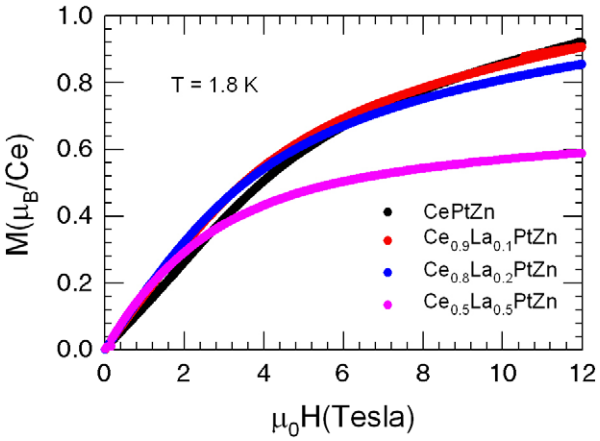

Figure 2. The magnetization of $Ce_{1-x}La_xPtZn$ ($x = 0$, 0.1, 0.2 and 0.5) at 1.8 K up to 12 T.

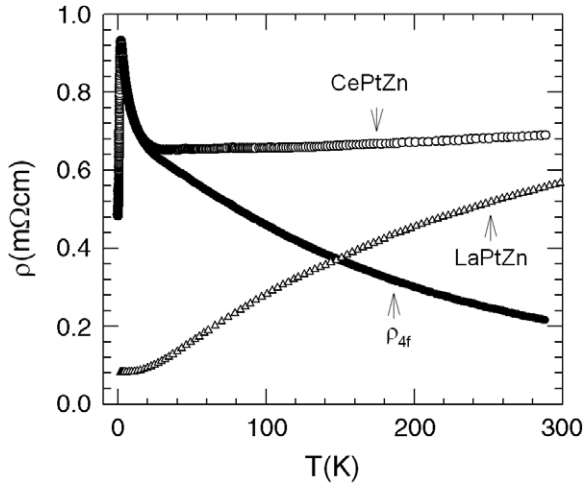

Figure 3. The zero field electrical resistivity of CePtZn between 60 mK and 300 K. For LaPtZn the resistivity data taken down to 1.8 K are plotted. $\rho_{4f}(=\rho_{CePtZn} - \rho_{LaPtZn})$ is also plotted.

moment $\mu_{eff} = 2.71$ and 2.81 μ_B, $\theta_p = -43.1$ and -52.4 K, $\chi_0 = 1.58 \times 10^{-3}$ and 1.46×10^{-3} emu mol^{-1} for the 100–300 K and 150–300 K ranges, respectively. These results can be taken to imply that the Ce ions in CePtZn are in the trivalent state with an antiferromagnetic exchange interaction between them. The slight deviation of μ_{eff} from the free Ce^{3+} ion value of 2.54 μ_B and a sizeable χ_0 is ascribed to the effect of CEF. The latter can also contribute to θ_p. A similar conclusion regarding the trivalent nature of Ce ions in CePtZn was arrived at in [4], which appeared during the course of this work and which reports a paramagnetic state of Ce ions in CePtZn, inferred from magnetization and heat capacity data taken down to 3 and 2 K, respectively. There is the hint of a peak in the susceptibility near 1.9 K (see the upper inset of figure 1) arising due to an antiferromagnetic phase transition. Since CePtZn crystallizes in a relatively low symmetry, orthorhombic structure, anisotropic behavior of the magnetization is quite plausible. A significant anisotropic behavior of the magnetization has been reported in the isostructural Kondo semiconductors CeNiSn [5] and CeRhSb [6].

For reasons given later, the susceptibility and the resistivity of a few alloys of composition $Ce_{1-x}La_xPtZn$ for $x = 0.1$, 0.2 and 0.5 were also measured. The curvature of χ^{-1} versus T seen in CePtZn is present for $x = 0.1$ and 0.2 to nearly the same degree (the data are not plotted for the sake of clarity), but it is reduced for $x = 0.5$, as seen in figure 1. For $x = 0.1$ and 0.2 the fitted values of μ_{eff} and θ_p again show minor variations with the temperature range in which the data are fitted, as for CePtZn, but μ_{eff} is close to the value for the free Ce^{3+} ion. For example, in $Ce_{0.8}La_{0.2}PtZn$, $\mu_{eff} = 2.6$ and 2.4 μ_B/Ce, $\theta_p = -30$ and -13.1 K, $\chi_0 = 2.12 \times 10^{-3}$ and 2.32×10^{-3} emu mol^{-1} for the 100–300 and 150–300 K ranges, respectively. The nearly linear variation of χ^{-1} versus T in $Ce_{0.5}La_{0.5}PtZn$ between 100 and 300 K furnishes $\mu_{eff} = 2.5$ μ_B/Ce, $\theta_p = -10$ K and $\chi_0 = 1.57 \times 10^{-4}$ emu mol^{-1}. Overall the negative θ_p decreases in its absolute value with the La dilution. Since CePtZn is a dense Kondo lattice (as inferred from the thermal variation of its resistivity, see below) there is a contribution to negative θ_p from the Kondo interaction. Substitution of Ce by La leads to a decrease of both the Kondo temperature (due to lattice expansion) and the T_N (due to dilution), which in turn is likely to lower the overall value of θ_p.

The isothermal magnetization per Ce ion of $Ce_{1-x}La_xPtZn$ alloys at 1.8 K measured up to 12 T is shown in figure 2. The relatively substantial value of the magnetization at 1.8 K reiterates the conclusion derived above that the Ce ions are in the trivalent state in these alloys. At the maximum applied field of 12 T, the magnetization, M, is maximum for CePtZn with a value of nearly 0.92 μ_B and decreases marginally for $x = 0.1$ and 0.2. However, for $Ce_{0.5}La_{0.5}PtZn$ the corresponding value of M is 0.6 μ_B. At low fields the magnetization of doped alloys is higher than that of CePtZn; this may be due to their lower T_N. Since the resistivity data in applied magnetic fields (see below) show that the T_N of CePtZn is close to zero at ∼6 T and the T_N of La-doped alloys should decrease due to the dilution, the antiferromagnetic ground state of these alloys does not affect the magnitude of the magnetization at high fields. The magnetization of the ground state is determined by the CEF but, since both La and Ce are notionally in the same trivalent charged state, the CEF effects most likely show minor variation with x in $Ce_{1-x}La_xPtZn$ alloys. The lower value of M for $x = 0.5$, suggests a possible concentration dependent effective Landé factor $g_{eff}(x)$. In $Ce_xLa_{1-x}Al_2$, for example, it has been inferred [7] that $|g_{eff}(x)|$ varies from 0.98 to 2.8 for $x = 0.015$ to 1, respectively, compared to the free Γ_7 doublet $|g|$ value of (10/7). The variation of g_{eff} with x has been ascribed to short range pair or cluster interaction between the Ce ions in $Ce_xLa_{1-x}Al_2$ which form at $x = 1$ a dense Kondo lattice, ordering antiferromagnetically at $T_N = 3.87$ K.

Figure 3 shows the electrical resistivity of CePtZn and the non-magnetic, reference analog LaPtZn. The 4f-contribution to the resistivity ρ_{4f} ($\rho_{4f} = \rho_{CePtZn} - \rho_{LaPtZn}$) is also plotted, assuming that the phonon contributions to the resistivities of LaPtZn and CePtZn are identical. The residual resistivity of LaPtZn (∼80 $\mu\Omega$ cm at 1.7 K) has also been subtracted from ρ_{CePtZn} in deriving ρ_{4f}. ρ_{CePtZn} and ρ_{LaPtZn} at room temperature are nearly 680 and 570 $\mu\Omega$ cm, respectively. These values

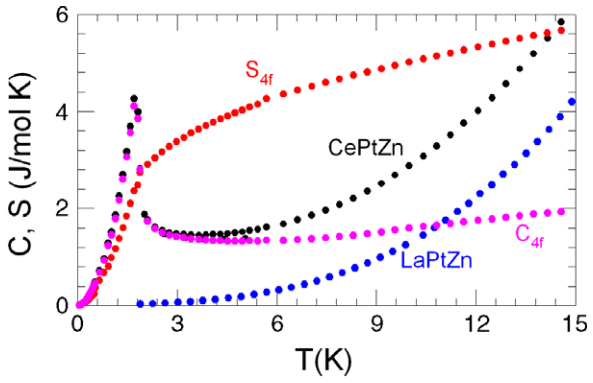

Figure 4. The heat capacity of CePtZn between 0.4 and 20 K. The heat capacity of the non-magnetic reference compound LaPtZn between 1.8 and 20 K is also plotted. $C_{4f}(=C_{CePtZn}-C_{LaPtZn})$ and the entropy S_{4f} obtained by integrating C_{4f}/T with respect to temperature are also plotted.

are higher than what is typically observed in intermetallic compounds. The corresponding values in YbPtZn and LuPtZn are 370 and 80 $\mu\Omega$ cm, respectively [1]. ρ_{CePtZn} shows minor variation with temperature down to about 30 K in sharp contrast to ρ_{LaPtZn}. Below 30 K ρ_{CePtZn} increases rapidly by nearly 0.3 mΩ cm, peaking broadly at 2 K, and then decreasing to a residual value of 0.48 mΩ cm at the lowest temperature of 60 mK in our experiment. The thermal variation of ρ_{4f} shows a negative temperature coefficient of resistivity from room temperature down to the peak at 2 K. On a logarithmic scale ρ_{4f} varies linearly with $-\ln T$ between room temperature and 100 K and between ~20 and 3 K with different slopes. Such a temperature dependence of ρ_{4f} indicates that CePtZn, like its Yb analog YbPtZn, is a dense Kondo lattice. The existence of two regions is explained as arising due to the incoherent Kondo scattering of the charge carriers from the fully six-fold degenerate Ce 4f level at high temperatures and from the CEF split electronic doublet ground state at low temperatures. In the orthorhombic symmetry of CePtZn the six-fold $J = 5/2$ state of the free Ce^{3+} ion will be split into three doublets, each of effective spin $S = 1/2$, by the crystal electric field. It may be recalled that the Kondo temperature depends on the degeneracy of the 4f level. The broad peak at 2 K represents the onset of correlations due to (i) the phase transition from a paramagnetic to a magnetically ordered state of the cerium ions near 1.7 K and (ii) the coherent Kondo scattering of the charge carriers in a periodic Kondo lattice. It indicates that the Kondo temperature associated with the CEF ground state is ~2 K.

Figure 4 shows the heat capacity of CePtZn measured in the range of 0.4–20 K. The heat capacity of the reference, non-magnetic compound, LaPtZn, measured between 1.8 and 20 K is also plotted. The heat capacity of CePtZn shows a peak at 1.7 K, with a peak height of nearly 4.4 J mol^{-1} K^{-1}, signifying a magnetic transition at that temperature. The peak height is substantially reduced compared to the mean field value of 12.5 J mol^{-1} K^{-1} for spin $S = 1/2$. The 4f-contribution to the specific heat C_{4f} and the corresponding entropy S_{4f} ($S_{4f} = \int_0^{T_c} \frac{C_{4f}}{T}$) is calculated by subtracting the heat capacity of LaPtZn from the heat capacity of CePtZn, assuming that the lattice contribution to the heat capacity is identical in the two compounds. The plot of the entropy S_{4f}, thus obtained, is also shown in figure 4. S_{4f} reaches a value of 2.4 J mol^{-1} K^{-1} at the transition temperature T_m, which is less than $R \ln 2$ (5.76 J mol^{-1} K^{-1}) for a doublet ground state with an effective spin $S = 1/2$. S_{4f} attains the latter value near 15 K. The nearly temperature independent behavior of C_{4f} above 4 K implies an increasing C_{4f}/T with a decrease of temperature in the paramagnetic regime. Such a behavior of C_{4f}/T much above T_m is typically seen in heavy fermion compounds with a low Kondo temperature, T_K, where the development of a many-body Abrikosov–Suhl resonance in the quasiparticle density of states gives rise to an increasing C/T with decreasing temperature. The zero field resistivity data discussed above clearly show that CePtZn is a dense Kondo lattice compound. However, the screening of the 4f-derived magnetic moment of the Ce ions in CePtZn by the many-body antiferromagnetically polarized electronic density of states is not complete and the Ce ions with reduced moments order magnetically at 1.7 K due to the indirect Ruderman–Kittel–Kasuya–Yosida (RKKY) exchange interaction. Extrapolating the C/T versus T^2 data between 0.8 and 0.4 K to $T = 0$ yields $C/T \sim 0.6$ J mol^{-1} K^{-2} as $T \to 0$, indicating large effective electronic masses. The corresponding value of γ for LaPtZn is 9.4 mJ mol^{-1} K^{-2} and the Debye temperature θ_D is 170 K. The two-fold degeneracy of the ground state is partially removed above T_m by the Kondo effect leading to reduced entropy. A simple calculation shows that $S_{mag}(T_m) = S_K(T_m/T_K)$, where S_{mag} is the entropy associated with the magnetic ordering and S_K is the entropy at T_m (=1.7 K) due to the Kondo effect [8]. Using the Bethe ansatz, the specific heat and the entropy for a spin 1/2 Kondo impurity have been calculated as a function of T/T_K [9]. The ratio T_m/T_K can thus be calculated using the value of S_{mag} (=S_{4f}). This simple procedure furnishes a value of 4.4 K for the single ion Kondo temperature T_K. A slightly higher T_K of 4.7 K is obtained if T_m is taken to be 2.2 K, the temperature at which the upturn in the heat capacity due to the magnetic ordering sets in. For a periodic lattice it is known that the Kondo coherence temperature $T_{coh} < T_K$. We have assumed vanishing short range magnetic correlations above T_m such that a reduced S_{mag} is solely ascribed to partial screening of the 4f moment by the Kondo interaction. Thus like its Yb analog, CePtZn is another example where the Kondo and magnetic interactions are of nearly equal strength.

The sharp increase of resistivity below 20 K, which varies as $\ln T$ down to 3 K is a feature that can qualitatively find an explanation in terms of the incoherent Kondo scattering of the charge carriers, as mentioned above. It was, however, noted that between 20 and 10 K the temperature dependence of $\rho(T)$ is represented well by $\rho(T) \propto \exp(\Delta/k_B T)$, with $\Delta \approx 4$ K, suggesting an activated behavior across a gap. It may be recalled that pseudo-gaps in the electronic density of states have been found in cerium based Kondo insulators such as $Ce_3Bi_4Pt_3$ [10], CeRhSb [11] and CeNiSn [12]; the last two compounds having the same crystal structure as CePtZn, as mentioned earlier. If a gap on the order of 4 K develops in CePtZn, then the resistivity at low temperatures should not show a peak and decrease significantly at lower

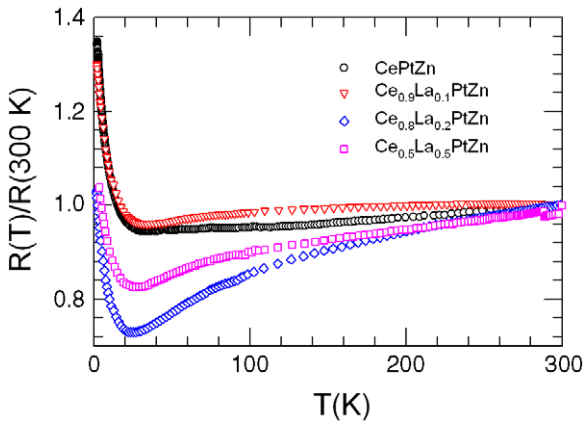

Figure 5. The electrical resistivity, $R(T)/R(300\ \mathrm{K})$ of $Ce_{1-x}La_xPtZn$ ($x = 0$, 0.1, 0.2, and 0.5) between 1.8 and 300 K.

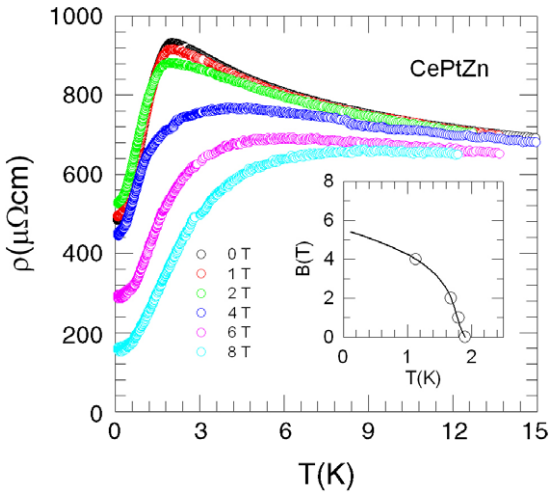

Figure 6. The electrical resistivity of CePtZn below 15 K in zero and applied fields up to 8 T. The inset shows the tentative phase diagram of T_N versus the applied magnetic field.

temperatures, unless the magnetic ordering at 1.7 K induces a metal to insulator transition as in UNiSn [13] or extrinsic effects dominate at low temperatures. The pseudo-ternary alloys $Ce_{1-x}La_xPtZn$ were primarily made to probe this aspect further, as the gap in Kondo insulators is known to depend sensitively on the lattice periodicity of rare earth ions, and even modest alloying destroys the activated behavior. A reduction in the gap by doping has been reported in $Ce_{3-x}La_xBi_4Pt_3$ [10], and other Kondo insulators. Figure 5 shows the resistivity $R(T)/R(300\ \mathrm{K})$ between 300 and 1.8 K of $Ce_{1-x}La_xPtZn$ for $x = 0$, 0.1, 0.2 and 0.5. The low temperature upturn is seen in all the alloys, even for $Ce_{0.5}La_{0.5}PtZn$. Minor substitution of Pt with Au and Ni (the data are not shown here) also does not qualitatively affect the low temperature upturn. Thus these doping studies show that the variation of resistivity with temperature in the range between 20 and 10 K in CePtZn which mimics a thermally activated behavior across a gap is just fortuitous and there is no pseudo-gap at low temperatures. The magnitude of resistivity at 300 K is 0.36, 1.15 and 0.17 mΩ cm for $x = 0.1$, 0.2 and 0.5, respectively. The resistivity of $x = 0.2$ alloy is larger than that of CePtZn in the entire temperature range between 1.8 and 300 K, while for $x = 0.1$ and 0.5 the absolute values decrease with La dilution. This apparent lack of a regular variation of resistivity with x may be due to extrinsic factors arising from micro-cracks in these alloys, which are quite brittle.

The resistivity data on CePtZn in zero and applied fields up to 8 T, from 15 K down to ∼60 mK, is shown in figure 6. The zero field resistivity peaks near 2 K and then decreases at lower temperatures as mentioned above. The peak temperature decreases in applied fields of 1 and 2 T and the magnetoresistivity becomes positive in the low temperature region. At higher applied fields the peak in the resistivity becomes broader and shifts to higher temperatures; to 9 K in a field of 8 T, for example. The inset of figure 6 shows the variation of T_N with the applied field B, obtained from $d\rho/dT$ versus T plots in a manner similar to that shown in the inset of figure 10(b) for the corresponding case of pressure. A region of negative magnetoresistance extends considerably below 12 K, reminiscent of similar behavior seen in Kondo lattice systems well above the coherence temperature. The positive magnetoresistivity below $T \sim 1.3$ K in applied fields of 1 and 2 T is mainly due to the greater positive contribution from the enhanced spin disorder, arising from the disrupting effect of the magnetic field on the antiferromagnetic alignment of the cerium magnetic moments. Since T_N is shifted to lower temperatures by applied fields and vanishes at around 5–6 T (see the inset of figure 6), the positive magnetoresistance is not observed at higher applied fields.

The resistivity follows the Fermi liquid behavior $\rho = \rho_0 + AT^n$ ($n = 2$) below ∼0.28 K in fields of $B = 0$, 1, 2 and 4 T, as shown by the solid lines in figure 7(a). The range of T^2 variation increases to 0.75 and 1.5 K in 6 and 8 T, respectively. On the other hand an exponent $n = 1.7$ provides a good fit to the data for $B = 4$ T up to nearly 0.9 K, as shown in figure 7(b.) The coefficient of the T^2 term, A, obtained by fitting the expression to the data decreases from 0 to 2 T, shows a maximum at 4 T, and decreases at higher fields. These results suggest that a quantum critical point is reached in CePtZn by tuning T_N to 0 with the external magnetic field, as seen earlier in the single crystals of $YbRh_2Si_2$ [14], YbAgGe [15] and $CeAuSb_2$ [16]. Data at intermediate fields between 4 and 6 T need to be taken to explore the thermal variation of resistivity in the low temperature region and the value of exponent n with field.

Another hallmark of the quantum critical point at which $T_N \to 0$ is the logarithmic divergence of the heat capacity, $\Delta C/T \propto -\ln T$, over a substantial temperature range. Heat capacity data on CePtZn were taken at 2, 4, 6 and 8 T, between 10 and 1.8 K, and they are shown in the inset of figure 8. Data below 1.8 K in applied fields could not be taken due to some technical problems experienced with a He^3 insert of PPMS. The main panel of figure 8 shows C_{4f}/T versus $\ln T$, obtained after subtracting the heat capacity of LaPtZn from the data at various fields. The upturn in the heat capacity due to the magnetic transition at 1.7 K has almost vanished at 4 T (see the inset) and the data show a decreasing trend at low temperatures at the higher fields of 6 and 8 T. A nearly

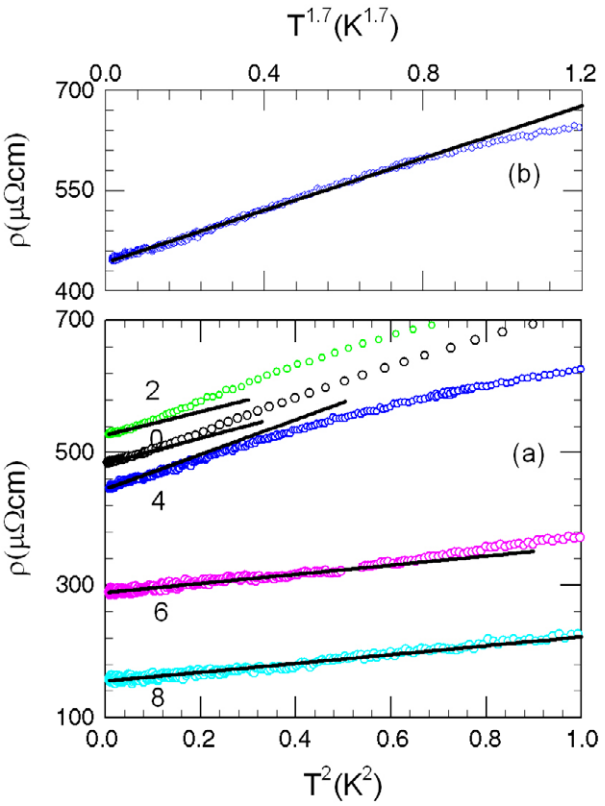

Figure 7. (a) ρ versus T^2 in various fields. The solid lines indicate the linear fitting at low temperatures, (b) the $T^{1.7}$ dependence of ρ up to 0.9 K at 4 T.

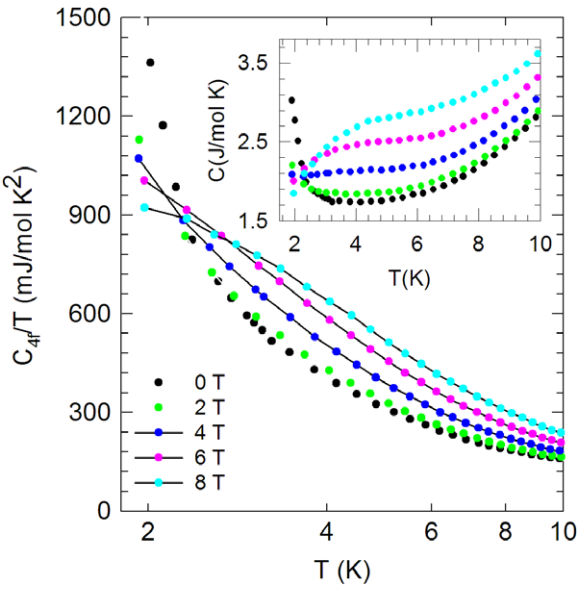

Figure 8. The heat capacity, C_{4f}, of CePtZn between 1.8 and 10 K in fields of 0, 2, 4, 6 and 8 T. The inset shows the total heat capacity C.

linear variation of C_{4f}/T versus $-\ln T$ between 7 and 1.8 K is observed at 6 T. Data at intermediate fields between 4 and 6 T and down to lower temperatures, preferably on single crystals, would be useful to establish more firmly the inference of a

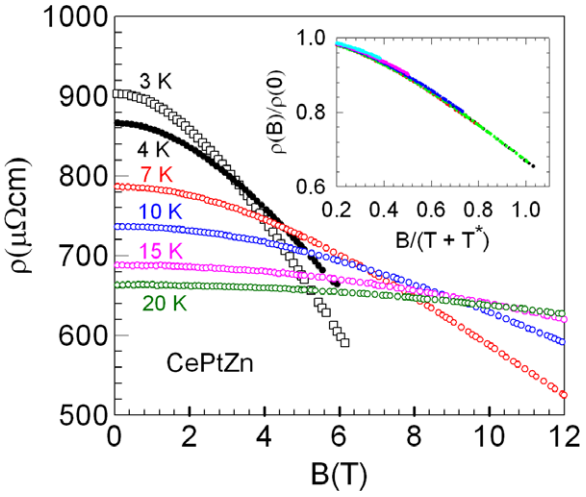

Figure 9. The electrical resistivity of CePtZn at 3, 4, 7, 10, 15 and 20 K up to 12 T. The inset shows the scaling behavior of the magnetoresistivity $\rho(B)/\rho(0)$ as a function of $B/(T + T^*)$.

field induced quantum critical point in CePtZn with potential magnetic anisotropy.

In the paramagnetic regime the negative contribution to the magnetoresistivity decreases with increasing temperature. Figure 9 shows the plots of ρ versus the field B at 3, 4, 7, 10, 15 and 20 K, where fields up to 12 T were employed at some temperatures. The magnetoresistivity varies as B^2 at low fields, the range of quadratic variation increasing as T is increased. Qualitatively, this agrees well with the expression derived by Horvatić and Zlatić [17], Okiji and Kawakami [18] for the magnetoresistivity of the single-orbital asymmetric Anderson model used to explain the electronic phenomena in dilute alloys, namely $\Delta\rho/\rho(0) = -D_0[1 - D_2(\pi k_B T/\Delta)^2/3]$ [17], where in the low field (B/Δ) limit (Δ is the finite line width of the impurity level) D_0 is proportional to B^2, while in the high field limit $D_0 \to 1$. D_2 has a maximum at $B = 0$ and drops quickly with increasing B. In the Kondo spin fluctuation regime of the Anderson model, $\Delta\rho/\rho(0)$ in the low-T and low-B regime is scaled by the same characteristic temperature T^*, which is an approximate measure of the Kondo temperature. Using the Bethe ansatz to solve the Coqblin–Schrieffer model, Schlottmann has shown [19] that, for a single-impurity Kondo interaction, the normalized magnetoresistivity $\rho(B)/\rho(0) = f(B/(T + T^*))$. The magnetoresistivity data of CePtZn measured at 3, 4, 7, 10, 15 and 20 K obey the scaling relation, as shown in the inset of figure 9 with a T^* of 1 K.

According to the well known Doniach phase diagram [20], in the interplay between the competing Kondo and the RKKY exchange interactions, the application of pressure favors a non-magnetic ground state, as it increases the hybridization between the 4f and the conduction electron states, thereby increasing T_K and decreasing T_N. Figure 10(a) shows the temperature dependence of ρ_{CePtZn} under high pressures up to 2.66 GPa (data were taken at some other values of pressure which are not shown for the sake of clarity). The arrow at ambient pressure indicates the temperature T_{max} where ρ exhibits a maximum. T_{max} increases gradually with increasing

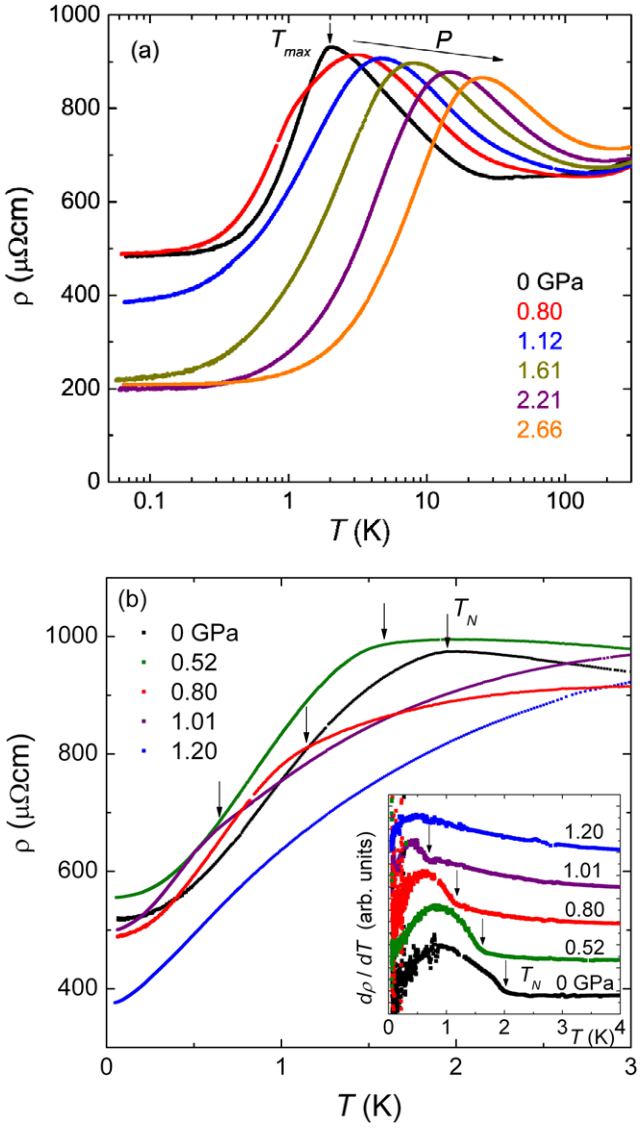

Figure 10. (a) Temperature dependence of ρ up to 2.66 GPa. (b) Low temperature part of ρ up to 1.20 GPa. The inset shows $d\rho/dT$ versus T to locate T_N. T_{max} increases and T_N decreases with increasing pressure.

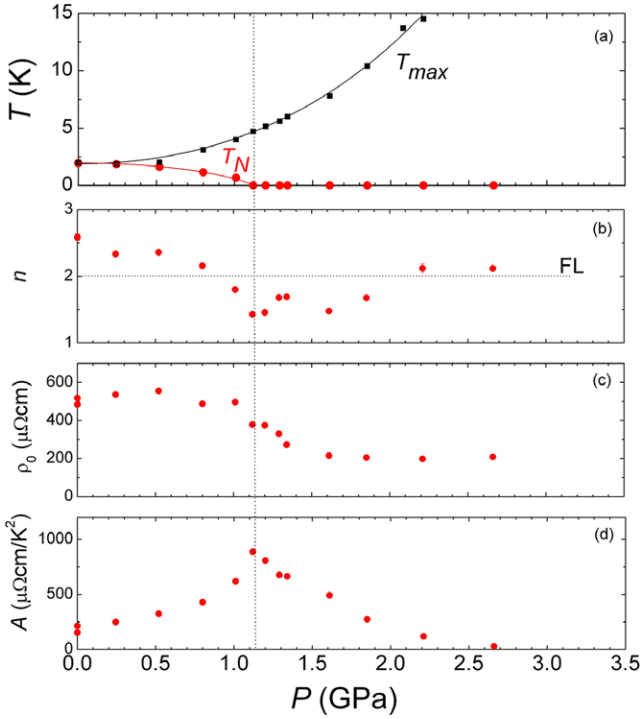

Figure 11. (a) Pressure–temperature phase diagram of CePtZn. ((b)–(d)) Pressure dependence of n, ρ_0 and A. T_N becomes zero around 1.2 GPa, accompanied with the peaking of A and the deviation from Fermi liquid behavior ($n = 2$).

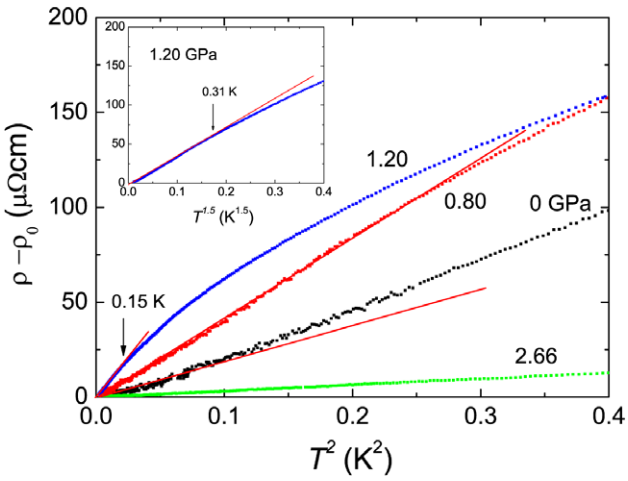

Figure 12. ρ–ρ_0 versus T^2. The solid lines indicate the linear fitting at low temperatures. The inset shows the $T^{1.5}$ dependence of ρ–ρ_0 up to 0.31 K at 1.20 GPa.

pressure, which is similar to the behavior seen in other archetypal Ce based Kondo lattice systems. Figure 10(b) shows the data below 3 K, in order to focus on the magnetic transition temperature T_N determined from the plots of $d\rho/dT$ versus T, as shown in the inset. Using this criterion, T_N is found to decrease with increasing pressure and vanish above 1.2 GPa. Therefore, the application of pressure induces a quantum critical point in CePtZn around 1.2 GPa.

Figure 11(a) displays the pressure–temperature phase diagram of CePtZn obtained from the data displayed in figures 10(a) and (b). Figures 11(b)–(d) show the pressure dependence of the exponent, n, the residual resistivity, ρ_0, and the coefficient, A, respectively. Here n is determined by using the formula $\rho = \rho_0 + AT^n$ for the data below 0.4 K, and A is determined by tentatively fitting the expression $\rho = \rho_0 + AT^2$ to the data at low temperatures in the range where such a dependence holds, as shown in figure 12. The coefficient A shows a clear peak around 1.2 GPa, which is the general trend at the quantum critical point as seen, for example, in Ce_7Ni_3 [21], $CePd_2Si_2$ [22], $CeIn_3$ [23] and $CeRhIn_5$ [24], where the quantum criticality was achieved by tuning the pressure. Simultaneously, the exponent n exhibits a minimum around 1.2 GPa, where it is estimated to be 1.5, as shown in the inset of figure 12, in conformity with the theoretical predictions [25] and reinforcing the conclusion that a quantum critical point exists at around 1.2 GPa. At pressures

higher than 2 GPa, the Fermi liquid behavior ($n = 2$) is recovered. The ρ_0 also shows a gradual decrease around 1.2 GPa. It may further be noted that the T_{max} at 1.2 GPa, where the magnetic state in CePtZn is completely suppressed, is approximately 5 K, which is lower than $T_{max} \sim 23$ K for $CeCu_2Si_2$ ($\gamma \sim 1$ J mol^{-1} K^{-2}) [26, 27] and $T_{max} \sim 15$ K for $CeCu_6$ ($\gamma \sim 1.6$ J mol^{-1} K^{-2}) [28, 29] at ambient pressure. The low $T_{max} \sim 5$ K for CePtZn indicates that a very heavy fermion state is realized around 1.2 GPa, as the value of γ is roughly inversely correlated with T_{max} in many heavy fermion compounds. Heat capacity measurements under pressure and in applied fields would be meaningful to find how the mass enhancement varies with pressure and magnetic fields, respectively. Measurements on a single crystal of CePtZn would be useful and illuminating, particularly with regard to the influence of anisotropy on the quantum critical point, the possible emergence of superconductivity near the pressure tuned quantum critical point, and a general comparison with results obtained on similar systems such as $YbRh_2Si_2$, $CeAuSb_2$, $CePd_2Si_2$, $CeIn_3$, $CeRhIn_5$, Ce_7Ni_3, etc.

To conclude, we have identified CePtZn as a heavy fermion Kondo lattice compound, which orders antiferromagnetically at 1.7 K, with a comparable Kondo temperature. The antiferromagnetic state is unstable against external magnetic fields and pressure. Our data indicate that a quantum critical point is reached in magnetic fields between 5 and 6 T at ambient pressure and at a pressure of 1.2 GPa in zero magnetic field.

References

[1] Dhar S K, Kulkarni R, Manfrinetti P, Pani M, Yonezawa Y and Aoki Y 2007 *Phys. Rev.* B **76** 054411
[2] Yvon K, Jeitschko W and Parthé E 1977 *J. Appl. Crystallogr.* **10** 73
[3] Kobayashi T C, Hidaka H, Kotegawa H, Fujiwara K and Eremets M I 2007 *Rev. Sci. Instrum.* **78** 023909
[4] Mishra R, Hermes W and Pöttgen R 2007 *Z. Naturf.* B **62** 1581
[5] Nakamoto G, Takabatake T, Fujii H, Minami A, Maezawa K, Oguro I and Menovsky A A 1995 *J. Phys. Soc. Japan* **64** 4834
[6] Takabatake T, Tanaka H, Bando Y, Fujii H, Nishigori S, Suzuki T, Fujita T and Kido G 1994 *Phys. Rev.* B **50** 623
[7] Bredl C D, Steglich F and Schotte K D 1978 *Z. Phys.* B **29** 327
[8] Mori H, Yashima H and Sato N 1985 *J. Low Temp. Phys.* **58** 513
[9] Desgranges H-U and Schotte K D 1982 *Phys. Lett.* A **91** 240
[10] Hundley M F, Canfield P C, Thompson J D and Fisk Z 1990 *Phys. Rev.* B **42** 6842
[11] Malik S K and Adroja D T 1991 *Phys. Rev.* B **41** 9607
[12] Takabatake T, Nakazawa Y and Ishikawa M 1987 *Japan. J. Appl. Phys.* **26** (Suppl. 26-3) 547
[13] Fujii H, Kawanaka H, Takabatake T, Kurisu M, Yamaguchi Y, Sakurai J, Fujiwara H, Fujita T and Oguro I 1989 *J. Phys. Soc. Japan* **58** 2495
[14] Gegenwart P, Custers J, Giebel C, Neumaier K, Tayama T, Tenya K, Trovarelli O and Steglich F 2002 *Phys. Rev. Lett.* **89** 056402
[15] Bud'ko S L, Morosan E and Canfield P C 2004 *Phys. Rev.* B **69** 014415
[16] Balicas L, Nakatsuji S, Lee H, Schlottmann P, Murphy T P and Fisk Z 2005 *Phys. Rev.* B **72** 064422
[17] Horvatić B and Zlatić V 1984 *Phys. Rev.* B **30** 6717
[18] Okiji A and Kawakami N 1982 *J. Phys. Soc. Japan* **51** 3192
[19] Schlottmann P 1983 *Z. Phys.* B **51** 223
[20] Doniach S 1977 *Valence Instabilities and Related Narrow-Band Phenomena* ed R D Parks (New York: Plenum) p 169
[21] Umeo K, Kadomatsu H and Takabatake T 1996 *J. Phys.: Condens. Matter* **8** 9743
[22] Raymond S and Jaccard D 2000 *Phys. Rev.* B **61** 8679
[23] Knebel G, Braithwaite D, Canfield P C, Lapertot G and Flouquet J 2001 *Phys. Rev.* B **65** 024425
[24] Knebel G, Aoki D, Brison J-P and Flouquet J 2008 *J. Phys. Soc. Japan* **77** 114704
[25] Moriya T and Takimoto T 1995 *J. Phys. Soc. Japan* **64** 960
[26] Steglich F, Aarts J, Bredl C D, Lieke W, Meschede D, Franz W and Schäfer H 1979 *Phys. Rev. Lett.* **43** 1892
[27] Bellarbi B, Benoit A, Jaccard D, Mignot J M and Braun H F 1984 *Phys. Rev.* B **30** 1182
[28] Stewart G R, Fisk Z and Wire M 1984 *Phys. Rev.* B **30** 482
[29] Thompson J D and Fisk Z 1985 *Phys. Rev.* B **31** 389